

Evidence of competing interactions within hole Fermi-surface sheets in the vicinity of KFe_2As_2

Y. Ota¹, K. Okazaki^{1,*}, Y. Kotani^{1,†}, T. Shimojima^{1,‡}, W. Malaeb¹, S. Watanabe², C.-T. Chen³, K. Kihou⁴, C. H. Lee⁴, A. Iyo⁴, H. Eisaki⁴, T. Saito⁵, H. Fukazawa⁵, Y. Kohori⁵, and S. Shin^{1,6,7}

¹*Institute for Solid State Physics (ISSP), University of Tokyo, Kashiwa, Chiba 277-8581, Japan*

²*Research Institute for Science and Technology, Tokyo University of Science, Chiba 278-8510, Japan*

³*Beijing Center for Crystal R&D, Chinese Academy of Science (CAS), Zhongguancun, Beijing 100190, China*

⁴*National Institute of Advanced Industrial Science and Technology (AIST), Tsukuba, Ibaraki 305-8568, Japan*

⁵*Department of Physics, Chiba University, Chiba 263-8522, Japan*

⁶*CREST, JST, Chiyoda-ku, Tokyo 102-0075, Japan*

⁷*RIKEN SPring-8 Center, Sayo-gun, Hyogo 679-5148, Japan*

(Dated: June 28, 2018)

We have investigated the superconducting(SC)-gap anisotropy of $\text{Ba}_{0.07}\text{K}_{0.93}\text{Fe}_2\text{As}_2$, $\text{Ba}_{0.12}\text{K}_{0.88}\text{Fe}_2\text{As}_2$, and $\text{Ba}_{0.24}\text{K}_{0.76}\text{Fe}_2\text{As}_2$ using laser-based angle-resolved photoemission spectroscopy. Whereas in the end material K122, the inner and middle Fermi surfaces (FSs) have substantially anisotropic SC gaps, the outer FS has an almost zero gap, and the middle FS has octet-line nodes, in the 7% Ba-doped sample, the SC gap of the inner FS becomes almost isotropic, the middle has a still anisotropic gap and nodes, and the outer has a finite gap and nodes. In addition, in the 12% and 24% Ba-doped samples, the SC gap of the middle FS becomes almost isotropic. We attribute this doping dependence to the existence of competing pairing interactions in this doping region.

PACS numbers: 74.25.Jb, 74.70.Xa, 71.18.+y, 79.60.-i

Superconductivity of iron-pnictides are induced by carrier doping in most cases. Hence, doping dependence of superconducting (SC) order parameter can reveal important character in the pairing interactions. Angle-resolved photoemission spectroscopy (ARPES) is a powerful tool for the direct observation of the SC gap, it has been extensively utilized to the iron-based superconductors [1] since their discovery. [2, 3] At the early stage, most of the ARPES studies reported the almost isotropic SC gap, although some thermodynamic properties have suggested anisotropic or nodal SC gaps. [4–6] Recently, several ARPES studies reported the anisotropic [7–9] and nodal [10, 11] SC gaps. Among the iron-based superconductors which have anisotropic and/or nodal SC gaps, $\text{Ba}_{1-x}\text{K}_x\text{Fe}_2\text{As}_2$ (BaK122) is particularly unique. K atom can be completely substituted for Ba site of the parent compound BaFe_2As_2 , and the end member KFe_2As_2 (K122) still shows a superconductivity with a critical temperature (T_c) = 3.4 K, whereas 40 % substitution is the optimal doping and the highest T_c of ~ 38 K can be obtained. The optimally-doped (OP) member has hole FS sheets around the Brillouin-zone (BZ) center (Γ point) and electron sheets around the BZ corner (X point), and the SC gaps of these FS sheets are fully gapped (no node in the SC gap). [1, 12] On the other hand, K122 had been suggested to have SC-gap nodes from several studies, [13–15] and its SC-gap symmetry had been proposed as a nodal s -wave [16, 17] or d -wave [18, 19] both experimentally and theoretically.

Laser-ARPES studies revealed that in the OP BaK122 the SC-gap anisotropies and FS-sheet dependence are weak for the three hole FSs around the BZ center, [20]

and that in K122 they are strong and the SC-gap nodes exist in the middle FS at the FS angle $\varphi \sim \pm 5^\circ$. [11] In addition, it has been found that the SC-gap size of the outer FS becomes abruptly reduced and vanishingly small for the overdoped (OD) region at the doping level where the electron FS at the BZ corner disappears ($x \sim 0.6$). [21]

Because the SC-gap anisotropies of K122 are significantly different from those of OP and OD BaK122 typically for the inner and middle FS sheets, it is very interesting to investigate how the SC-gap anisotropies of three hole FS sheets around BZ center change with Ba doping from K122. We have measured SC-gap sizes of 7 % Ba-doped sample $\text{Ba}_{0.07}\text{K}_{0.93}\text{Fe}_2\text{As}_2$ (BaK0.93, $T_c \sim 7$ K), 12 % Ba-doped sample $\text{Ba}_{0.12}\text{K}_{0.88}\text{Fe}_2\text{As}_2$ (BaK0.88, $T_c \sim 13$ K) and 24 % Ba-doped sample $\text{Ba}_{0.24}\text{K}_{0.76}\text{Fe}_2\text{As}_2$ (BaK0.76, $T_c \sim 17$ K) using a low-temperature high-resolution laser-ARPES apparatus that achieves the highest energy resolution of $70 \mu\text{eV}$ and the lowest temperature of 1.5 K. [11], and find that the SC-gap anisotropies of three hole FS sheets drastically change with a small amount of Ba doping. In addition, although the SC-gap sizes of the outer FS were vanishingly small for K122 and $\text{Ba}_{0.3}\text{K}_{0.7}\text{Fe}_2\text{As}_2$ (BaK0.7), [21] those of BaK0.93, BaK0.88, and BaK0.76 show strong anisotropies and nodes exist for these compounds. On the other hand, for the middle FS, whereas SC-gap nodes exist for BaK0.93, the anisotropy is strongly suppressed for BaK0.88 and BaK0.76. We attribute this drastic doping dependence to the existence of the competing interactions as Maiti *et al.* proposed that the intraband and interband interactions are nearly degenerate. [22]

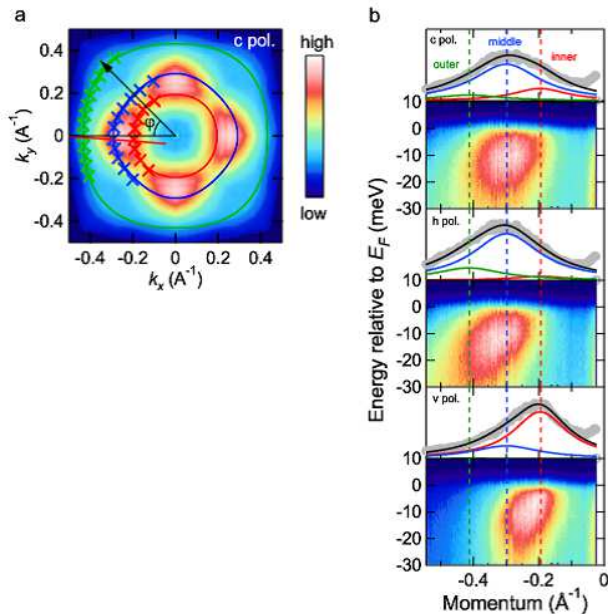


FIG. 1: FS map and MDCs at E_F for BaK0.93. (a) FS map measured with c -polarized light. The integration energy window is ± 5 meV from E_F . The image is symmetrized assuming a crystal tetragonal symmetry. Red, blue, and green markers indicate the positions of k_F for inner-, middle-, and outer-hole FSs, respectively. Definition of the FS angle φ is shown. (b) MDCs at E_F and E - k maps obtained with c -, h -, and v -polarized light for $\varphi \sim 0^\circ$ as indicated by the red line in (a). In these measurements, we used the experimental configurations similar to the previous study of K122. [11]

High quality single crystals were grown by self-flux method with KAs flux as described in Ref. 23. Clean surfaces were obtained by cleaving the sample *in situ* under ultra-high vacuum better than 5×10^{-11} Torr. ARPES data were collected using the laser-ARPES apparatus at ISSP with the 6.994 eV, 6th harmonics of Nd:YVO₄ quasi-continuous wave (q-CW, repetition rate = 240 MHz) laser and VG-Scienta HR8000 electron analyzer as described in Ref. 11. The overall energy resolution was set to ~ 1.2 meV for the SC-gap measurements and ~ 4 meV for the FS and E - k maps, and the angular resolution was 0.1 deg. Polarization of the incident excitation laser was adjusted using half-wave ($\lambda/2$) and quarter-wave ($\lambda/4$) plates. The superconducting transition temperatures were determined by the magnetization measurements before and after the ARPES measurements. The temperature dependence of the ARPES spectra were consistent with the magnetization measurements (see Fig. S1).

First, we determined the positions of Fermi momentum (k_F) for three (inner, middle, and outer) hole FSs around the BZ center. The FS map of BaK0.93 is shown in Fig. 1a. This FS map was measured with circularly(c)-polarized light and symmetrized by assuming the tetrag-

TABLE I: Fitting parameters for k_F positions using equation (1) and cross-sectional FS area. The areas are expressed as a percentage of the area of the 2D BZ.

inner			
x	k_{F0}	A	area
1	0.22	0.02	5.9
0.93	0.20	-0.02	4.7
0.88	0.18	-0.06	3.9
0.76	0.17	0.01	3.6
middle			
x	k_{F0}	A	area
1	0.30	0.053	10.6
0.93	0.29	0.031	10.1
0.88	0.28	0.004	9.5
0.76	0.25	0.03	7.5
outer			
x	k_{F0}	A	area
1	0.46	-0.02	24.8
0.93	0.44	-0.07	23.2
0.88	0.44	-0.05	22.9
0.76	0.43	-0.04	22.2

onal crystal structure (see Fig. S2 for raw data and other polarizations). The momentum distribution curves (MDCs) at E_F and E - k maps are shown in Fig. 1b, measured with the c -, horizontally(h)- and vertically(v)-polarized light [11] for $\varphi \sim 0^\circ$. The k_F positions of three hole FSs were determined by fitting to the three Lorentzians as in the case of K122, and are indicated by the symbols on the FS map in Fig. 1a. The polarization dependence of these MDCs is similar to that of K122, and thus the dominant orbital character of each FS sheet also should be similar to that of K122, i.e., the inner, middle, and outer FSs are dominantly contributed from xz/yz , $xz/yz + z^2$, and $x^2 - y^2$ orbitals, respectively. We fitted the k_F positions to the following model function,

$$k_F(\varphi) = k_{F0}[1 + A \cos(4\varphi)]. \quad (1)$$

From this fitting, we got the cross-sectional area of each FS sheet. With the same procedures, we determined the k_F positions and FS areas for BaK0.88 and BaK0.76 (Figs. S3-S5). The results are shown in Table I. The doping dependence of the FS areas is consistent with the nominal change of the Fe valence.

The energy distribution curves (EDCs) measured below T_c and above T_c are shown in Fig. 2 for BaK0.93 and BaK0.88. Figures 2a-2c show the EDCs at k_F of the inner, middle, and outer FSs, respectively, for BaK0.93 ($T_c \sim 7$ K) measured at 1.5 K (below T_c) and 10 K (above T_c). Each EDC at k_F is identified with a FS angle φ (Fig. 1). The EDCs shown in Fig. 2a-2c were symmetrized with respect to E_F , and the results are shown in Fig. 2d-2f, respectively. For the inner FS, the EDCs at k_F clearly show the superconducting coherence peaks, and the anisotropy of the SC-gap size seem to be rather

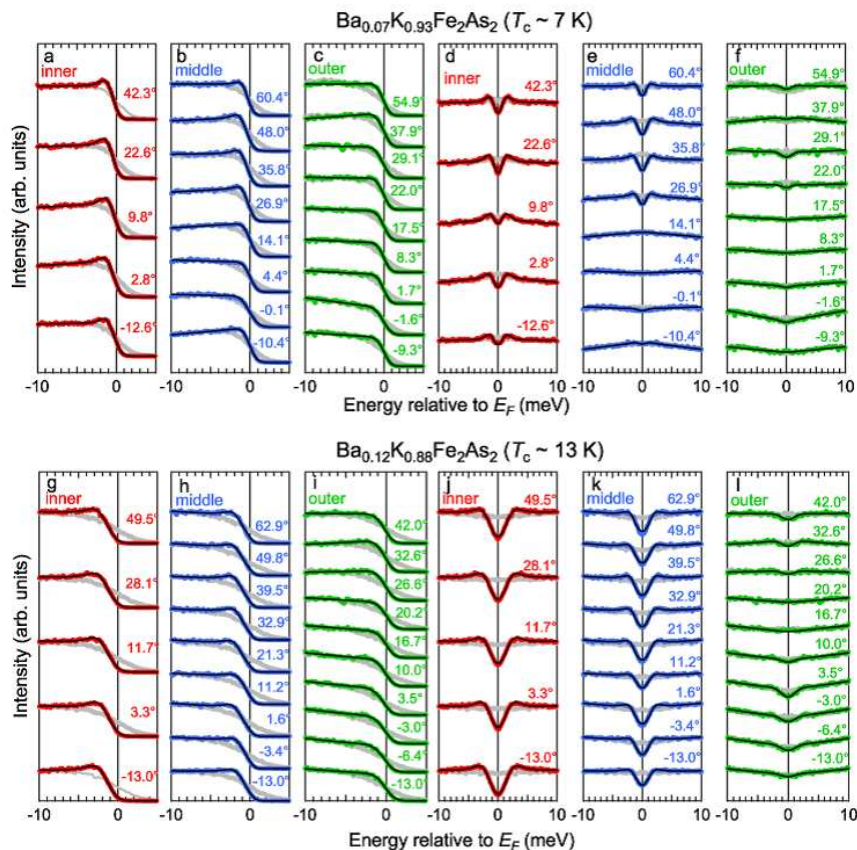


FIG. 2: EDCs and symmetrized EDCs at k_F measured below T_c and above T_c . (a)-(c) EDCs at k_F of inner (a), middle (b), and outer FSs (c), respectively, for BaK0.93 measured at 1.5 K and 10 K ($T_c \sim 7$ K) for various FS angles as shown in each panel. (d)-(f), Symmetrized EDCs of inner (d), middle (e), and outer FSs (f), respectively. (g)-(i), EDC at k_F of inner (g), middle (h), and outer FSs (i), respectively, for BaK0.88 measured at 1.5 K and 16 K ($T_c \sim 13$ K). (j)-(l), Symmetrized EDCs of inner (j), middle (k), and outer FSs (l), respectively. Gray markers indicate the EDCs above T_c and the solid lines indicate the fitting functions using a BCS spectral function. The results for BaK0.76 are shown in Fig. S6.

small. For the middle FS, the line shape of the symmetrized EDCs at k_F is strongly dependent on the FS angle in the vicinity of E_F , indicating that the SC gap is highly anisotropic. For the outer FS, the behavior of the symmetrized EDCs are similar to the middle FS. Thus, there is a FS-sheet dependence in the SC-gap sizes of BaK0.93 as in K122. However, a significant difference exists for the outer FS, where the SC-gap size is almost zero for all FS angles for the case of K122. Figures 2g-2i show the EDCs at k_F of the inner, middle, and outer FSs, respectively, for BaK0.88 ($T_c \sim 13$ K) measured at 1.5 K (below T_c) and 16 K (above T_c). The symmetrized EDCs are shown in Figs. 2g-2i. The anisotropy of the SC-gap size in the middle FS is different from those of K122 and BaK0.93, where the strong anisotropy exists, but similar to that of the OP BaK122, where the anisotropy is weak. For the outer FS, the symmetrized EDCs in Fig. 2l indicate that the SC gap has a strong anisotropy and nodes may exist. This sheet dependence is also different from the other doping levels, OP BaK122, BaK0.93, and

K122. The results for BaK0.76 are shown in Fig. S6, and the overall FS-sheet dependence and anisotropy of the SC gap are similar to those of BaK0.88.

In order to quantify the SC-gap size, we have fitted the EDCs to the BCS spectral function. [11] All the EDCs at 1.5 K could be fitted to the calculated spectra, as shown by the solid lines in Fig. 2. We plot the SC-gap sizes derived from fitting as a function of FS angle φ in Fig. 3 for BaK0.93 (Fig.3a), BaK0.88 (Fig.3b), and BaK0.76 (Fig.3c) as indicated by the solid circles. The open circles are plotted by symmetrizing data, taking into account the tetragonal crystal symmetry. To obtain insight into the SC-gap anisotropy, we have tried to fit the SC gaps with the two lowest harmonics under the fourfold tetragonal symmetry,

$$\Delta(\varphi) = |\Delta_0 + \Delta_4 \cos(4\varphi) + \Delta_8 \cos(8\varphi)|, \quad (2)$$

as in the case of K122. Whereas a $\cos(8\varphi)$ term was finite in the case of K122, we confirmed that the $\cos(8\varphi)$ component is unnecessary to reproduce the SC-

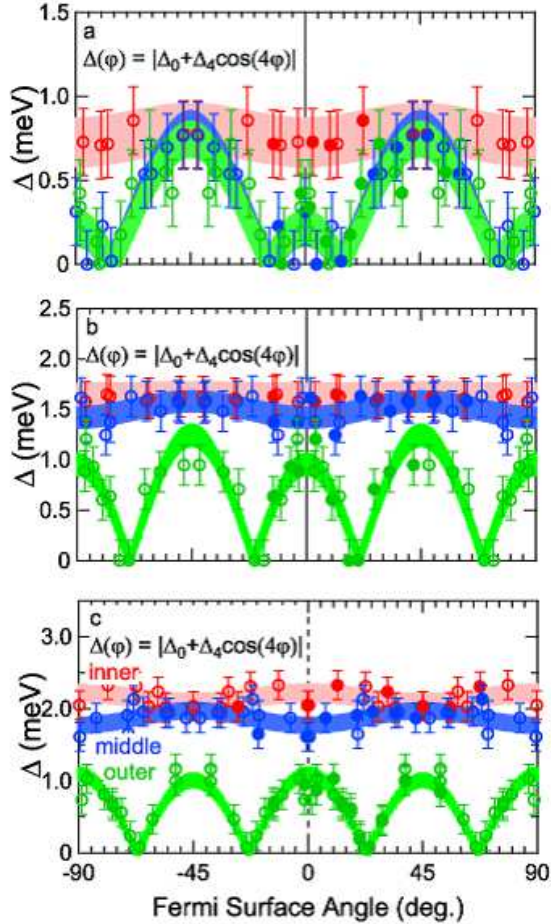


FIG. 3: Anisotropy of SC gaps and fitting results for each FS. (a)-(c), SC-gap sizes derived from the fitting using a BCS spectral function plotted as a function of FS angle for BaK0.93 (a), BaK0.88 (b), and BaK0.76 (c), respectively. The solid circles are derived from the EDCs shown in Fig. 2 and the open circles are plotted by symmetrizing taking into account the tetragonal crystal symmetry. The error bar for the plots denotes the standard deviation of the E_F position. The thick lines are the fitting functions using a model gap function of $\Delta(\varphi) = |\Delta_0 + \Delta_4 \cos(4\varphi)|$. The line width corresponds to the standard deviation of the fitting function.

gap anisotropy of the measured three compounds of BaK0.93, BaK0.88, and BaK0.76. Thus, we omitted the $\cos(8\varphi)$ term. The fitting is successful for these three compounds as shown in Fig. 3. First of all, the SC-gap symmetry of these three compounds should be A_{1g} type (s -wave) as in the case of K122, because the inner FS has no SC-gap nodes. In addition, the anisotropy is strongly suppressed in comparison to K122, where the $\cos(8\varphi)$ component can be recognized. As for the middle FS, the SC-gap nodes exist for BaK0.93, as in the case of K122, and they are determined to be located at $\varphi = \pm(16.0 \pm 2.3)^\circ$. On the other hand, for the cases

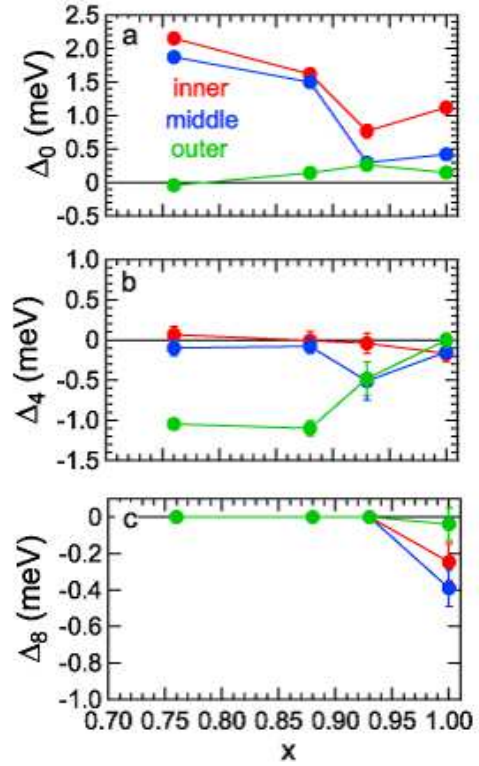


FIG. 4: Figure 4 | Doping dependence of fitting parameters for Fig. 3. (a) isotropic component Δ_0 , (b) $\cos(4\varphi)$ component Δ_4 , and (c) $\cos(8\varphi)$ component Δ_8 , respectively.

of BaK0.88 and BaK0.76, the anisotropy is strongly suppressed. Finally for the outer FS, strong anisotropies exist for these three compounds, in strong contrast to K122 and BaK0.7, where the SC gaps of the outer FS were vanishingly small. The SC-gap nodes also exist in the outer FS for these three compounds and they are determined to be located at $\varphi = \pm(15.2 \pm 2.8)^\circ$ for BaK0.93, $\varphi = \pm(22.2 \pm 0.4)^\circ$ for BaK0.88, and $\varphi = \pm(20.2 \pm 1.8)^\circ$ for BaK0.76, respectively.

Figure 4a-4c show the doping dependence of the fitting parameters of Δ_0 , Δ_4 , and Δ_8 , respectively, for the inner, middle, and outer FSs (see Fig. S7 for the ratio to $k_B T_c$, where k_B is the Boltzmann constant). First, the doping dependence of the isotropic component Δ_0 seems to be not so systematic. Those of the inner and middle FSs are rather small for BaK0.93 compared to the other compounds. That of the outer FS is slightly larger for BaK0.93. As for the $\cos(4\varphi)$ component Δ_4 , that of the inner FS is very small for all the compounds. On the other hand, that of the middle FS is large only for the case of BaK0.93. For the case of the outer FS, Δ_4 becomes monotonically larger by Ba doping from K122 to BaK0.88 and it becomes slightly small at BaK0.76. Finally, the $\cos(8\varphi)$ component Δ_8 is finite only for K122.

At first glance, this doping dependence may seem to

be inconsistent with the OP BaK122 and even with OD BaK122, because the OP BaK122 has almost isotropic SC gaps and the SC-gap size of the outer FS is vanishingly small for BaK0.7. [21] However, if Δ_4 of the outer FS becomes almost zero by further Ba doping, it is completely consistent with BaK0.7. It should be possible because Δ_4 of the middle FS becomes almost zero at BaK0.88 although that of BaK0.93 is rather large. We attributed this doping dependence of SC gap to the existence of competing pairing interactions. Recently, Maiti *et al.* proposed that if the intraband and interband interactions of the hole FSs are nearly degenerate, the existence of the SC-gap nodes in the middle FS of K122 can be reproduced. [22] From our results, the components of Δ_0 , Δ_4 , and Δ_8 change rather drastically with the small amount of Ba doping. This should indicate that two kinds of interactions are nearly degenerate and competing in this doping region, as Maiti *et al.* proposed that the interband and intraband interactions are nearly degenerate to explain the octet nodal behavior of K122. [22] It can be regarded that because two kinds of interactions are competing in this doping region, the SC-gap anisotropy is very sensitive to the small amount of Ba doping.

If the origin of the competing interactions are interband and intraband interactions as proposed by Maiti *et al.*, it is suggested that both of the spin and orbital fluctuations are important. Because the orbital contribution for the outer FS is almost only from the $x^2 - y^2$ orbital, [11, 20] the interband and intraband interactions for this band is inter-orbital and intra-orbital interactions, respectively. In addition, spin and orbital fluctuations can be considered as the origin of these interactions and they are intra-orbital and inter-orbital interactions, [24, 25] respectively. Thus, both of the spin and orbital fluctuations seem to be important at the same level at least for the outer FS.

We have investigated the anisotropy of superconducting (SC) gap for several Ba-doped KFe_2As_2 (K122) samples using laser-based angle-resolved photoemission spectroscopy. A drastic change is observed in the SC-gap anisotropy and nodal behaviors with a small amount of Ba doping. We attribute this drastic doping dependence to the existence of competing pairing interactions in this doping region. From this competition, it is suggested that both of the spin and orbital interactions are impor-

tant as the origin of the pairing interactions.

We would like to thank Y. Matsuda, T. Shibauchi, H. Kontani, R. Arita, and H. Ikeda for valuable discussions and comments. This research is supported by Grant-in-Aid for JSPS Fellows 23-6478, and JSPS through its FIRST Program.

* Present address: Department of Physics, University of Tokyo, Tokyo 113-0033, Japan

† Present address: Japan Synchrotron Radiation Research Institute (JASRI/SPring-8), Sayo, Hyogo 679-5198, Japan

‡ Present address: Department of Applied Physics, University of Tokyo, Tokyo 113-8656, Japan

- [1] H. Ding *et al.*, Europhys. Lett. **83**, 47001 (2008).
- [2] Y. Kamihara, T. Watanabe, M. Hirano, and H. Hosono, J. Am. Chem. Soc **130**, 3296 (2008).
- [3] M. Rotter, M. Tegel, and D. Johrendt, Phys. Rev. Lett. **101**, 107006 (2008).
- [4] K. Hashimoto *et al.*, Phys. Rev. B **81**, 220501 (2010).
- [5] B. Zeng *et al.*, Nat. Commun. **1**, 112 (2010).
- [6] M. Yamashita *et al.*, Phys. Rev. B **84**, 060507 (2011).
- [7] K. Umezawa *et al.*, Phys. Rev. Lett. **108**, 037002 (2012).
- [8] S. V. Borisenko *et al.*, Symmetry **4**, 251 (2012).
- [9] K. Okazaki *et al.*, Phys. Rev. Lett. **109**, 237011 (2012).
- [10] Y. Zhang *et al.*, Nat. Phys. **8**, 371 (2012).
- [11] K. Okazaki *et al.*, Science **337**, 1314 (2012).
- [12] K. Nakayama *et al.*, Europhys. Lett. **85**, 67002 (2009).
- [13] H. Fukazawa *et al.*, J. Phys. Soc. Jpn **78**, 083712 (2009).
- [14] J. K. Dong *et al.*, Phys. Rev. Lett. **104**, 087005 (2010).
- [15] K. Hashimoto *et al.*, Phys. Rev. B **82**, 014526 (2010).
- [16] H. Kawano-Furukawa *et al.*, Phys. Rev. B **84**, 024507 (2011).
- [17] K. Suzuki, H. Usui, and K. Kuroki, Phys. Rev. B **84**, 144514 (2011).
- [18] J.-P. Reid *et al.*, Phys. Rev. Lett. **109**, 087001 (2012).
- [19] R. Thomale, C. Platt, W. Hanke, J. Hu, and B. A. Bernevig, Phys. Rev. Lett. **107**, 117001 (2011).
- [20] T. Shimojima *et al.*, Science **332**, 564 (2011).
- [21] W. Malaeb *et al.*, Phys. Rev. B **86**, 165117 (2012).
- [22] S. Maiti, M. M. Korshunov, and A. V. Chubukov, Phys. Rev. B **85**, 014511 (2012).
- [23] K. Kihou *et al.*, J. Phys. Soc. Jpn. **79**, 124713 (2010).
- [24] K. Kuroki, S. Onari, R. Arita, H. Usui, Y. Tanaka, H. Kontani, and H. Aoki, Phys. Rev. Lett. **101**, 087004 (2008).
- [25] H. Kontani and S. Onari, Phys. Rev. Lett. **104**, 157001 (2010).

Supplemental Material for “Evidence of competing interactions within hole Fermi-surface sheets in the vicinity of KFe_2As_2 ”

Y. Ota¹, K. Okazaki^{1,*}, Y. Kotani^{1,†}, T. Shimojima^{1,‡}, W. Malaeb¹,
S. Watanabe², C.-T. Chen³, K. Kihou⁴, C. H. Lee⁴, A. Iyo⁴,
H. Eisaki⁴, T. Saito⁵, H. Fukazawa⁵, Y. Kohori⁵, and S. Shin^{1,6,7}

¹*Institute for Solid State Physics (ISSP),*

University of Tokyo, Kashiwa, Chiba 277-8581, Japan

²*Research Institute for Science and Technology,*

Tokyo University of Science, Chiba 278-8510, Japan

³*Beijing Center for Crystal R&D, Chinese Academy of Science (CAS),*

Zhongguancun, Beijing 100190, China

⁴*National Institute of Advanced Industrial Science and*

Technology (AIST), Tsukuba, Ibaraki 305-8568, Japan

⁵*Department of Physics, Chiba University, Chiba 263-8522, Japan*

⁶*CREST, JST, Chiyoda-ku, Tokyo 102-0075, Japan*

⁷*RIKEN SPring-8 Center, Sayo-gun, Hyogo 679-5148, Japan*

I. TEMPERATURE-DEPENDENT SYMMETRIZED EDCS

Figures S1 show the temperature dependence of symmetrized EDCs at k_F of the inner FS for BaK0.93, BaK0.88 and BaK0.76. These results are consistent with T_c determined by the magnetization measurements.

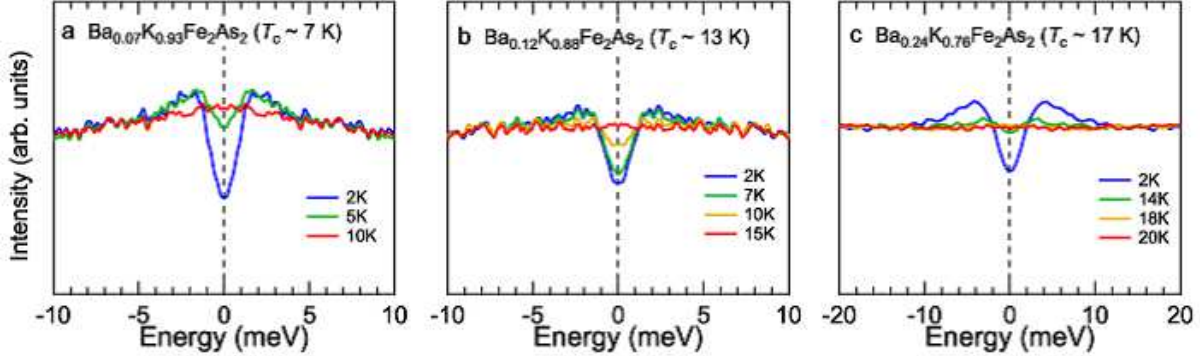


FIG. S 1: Temperature-dependent symmetrized EDCs for BaK0.93, BaK0.88 and BaK0.76. (a)-(c) Temperature-dependence of symmetrized EDCs at k_F of the inner FS for BaK0.93(a), BaK0.88(b) and BaK0.76(c) from the lowest temperature to above T_c .

II. POLARIZATION-DEPENDENT FS MAPS AND DETERMINATION OF k_F POSITIONS

Figures S2-S4 show the raw FS images plotted with respect to detector and rotation angles (a)-(c) and momentum-mapped FS images (d)-(e) for BaK0.93, BaK0.88 and BaK0.76, respectively. The integration energy window is ± 5 meV from E_F , the same as that for Fig. 1a. k_F positions were determined from the peak positions of those measured with c - and h - , and v -polarized light as indicated by the symbols. The determined k_F positions were confirmed to obey the fourfold tetragonal symmetry of the crystal structure.

III. POLARIZATION-DEPENDENT MDCS AND E - k MAPS

Figures S5a and S5b show the MDCs at E_F and E - k maps measured with c - , h - , and v -polarized light for BaK0.88 and BaK0.76, respectively. Momentum cuts are indicated by

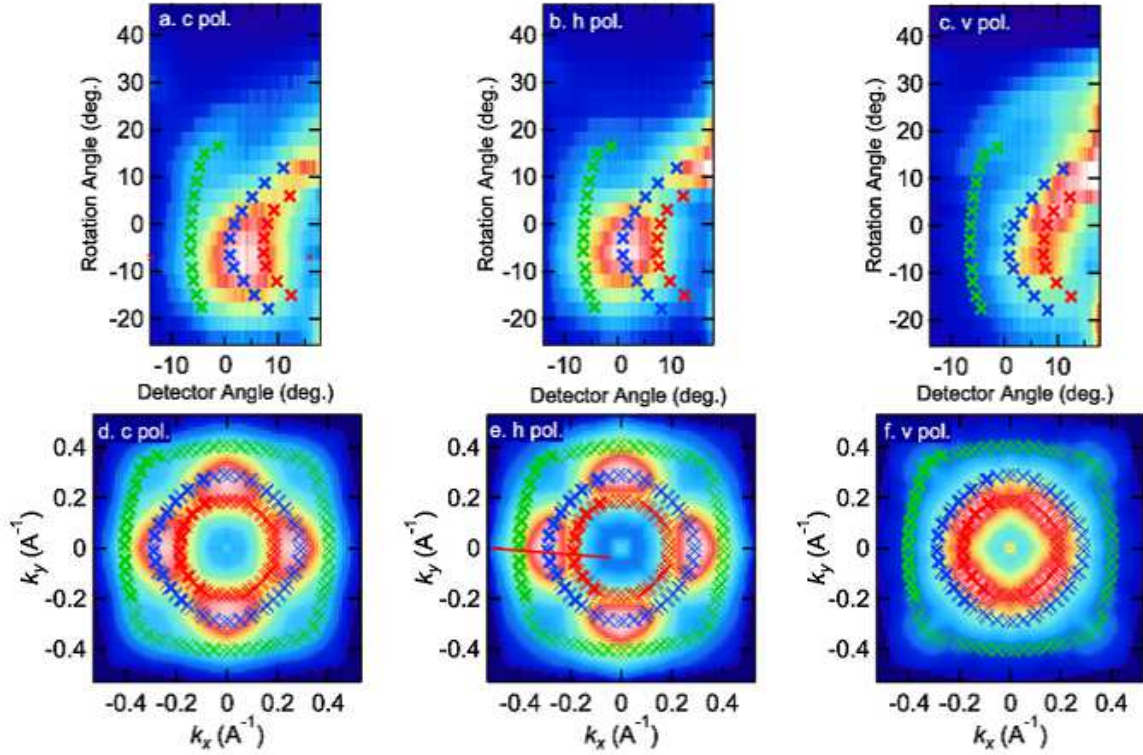


FIG. S 2: Polarization dependence of the FS map for BaK0.93. (a)-(c) Raw FS images plotted with respect to detector and rotation angles measured with c -, h -, and v -polarized light, respectively, and (d)-(f) momentum-mapped FS images.

the red lines in the panel e of Figs. S3 and S4, respectively. k_F positions of three hole FSs (inner, middle, and outer) were determined by fitting to the three Lorentzians, as in the cases of K122 and BaK0.93, and are indicated by the symbols on the FS maps in Figs. S3 and S4. The polarization dependence of these MDCs is similar to that of K122, and thus dominant orbital character of each FS sheet is also similar to that of K122.

IV. SC-GAP ANISOTROPIES OF BAK0.76

Figure S6 show the EDCs (a-c) and symmetrized EDCs (d-f) at k_F of the inner, middle and outer FSs measured below T_c (1.5 K) and above T_c (18 K) for BaK0.76 ($T_c \sim 17$ K). Each EDC at k_F is identified with FS angle φ (Fig. 1a). As in the case of BaK0.88, the EDCs at k_F of the inner and middle FSs clearly show superconducting coherence peaks, and

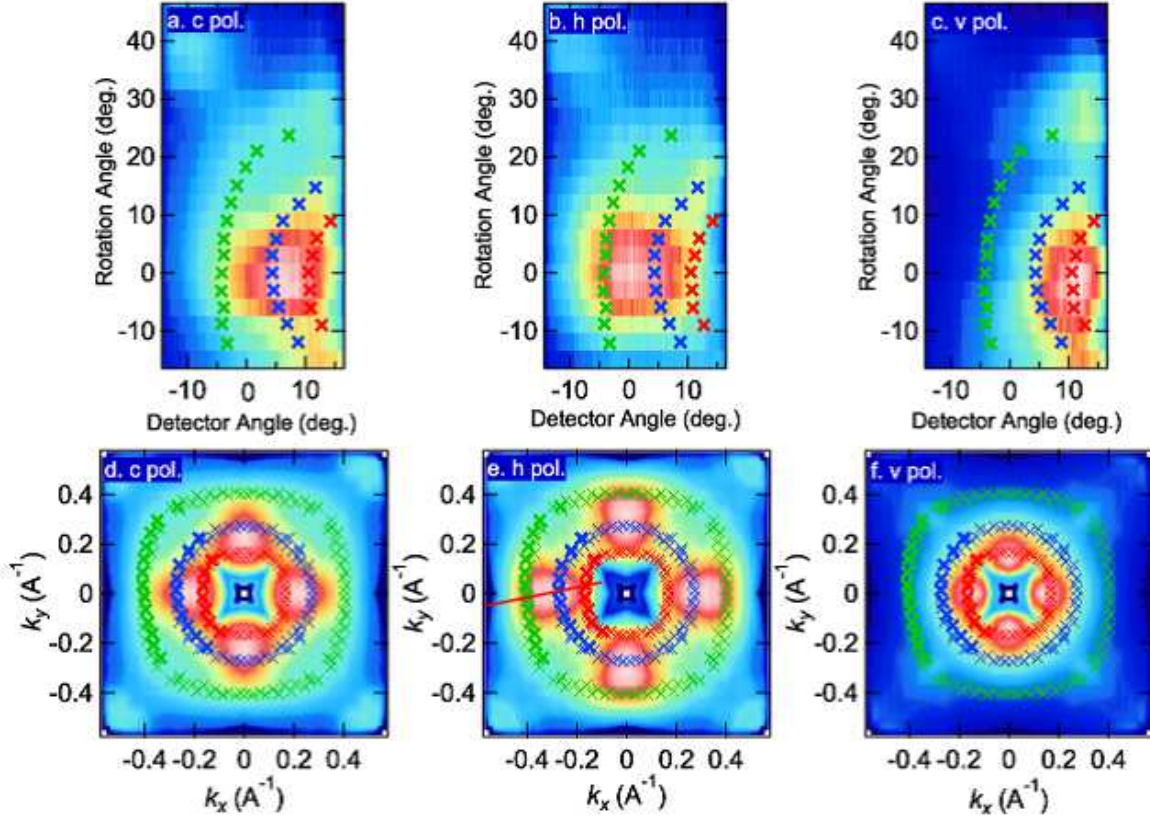


FIG. S 3: Polarization dependence of the FS map for BaK0.88. (a)-(c) Raw FS images plotted with respect to detector and rotation angles measured with c -, h -, and v -polarized light, respectively, and (d)-(f) momentum-mapped FS images.

the anisotropy of the SC-gap size seem to be rather small. For the outer FS, the symmetrized EDCs in Fig. S6f indicate that the SC gap has a strong anisotropy and nodes exist. This FS sheet dependence is similar to that of the BaK0.88.

V. DOPING DEPENDENCE OF $2\Delta/k_B T_c$

Figure S7 shows a doping dependence of $2|\Delta_0|/k_B T_c$ (a), $2|\Delta_4|/k_B T_c$ (b) and $2|\Delta_8|/k_B T_c$ (c), respectively. Δ_4 of the middle FS is drastically suppressed at BaK0.88 compared to BaK0.93.

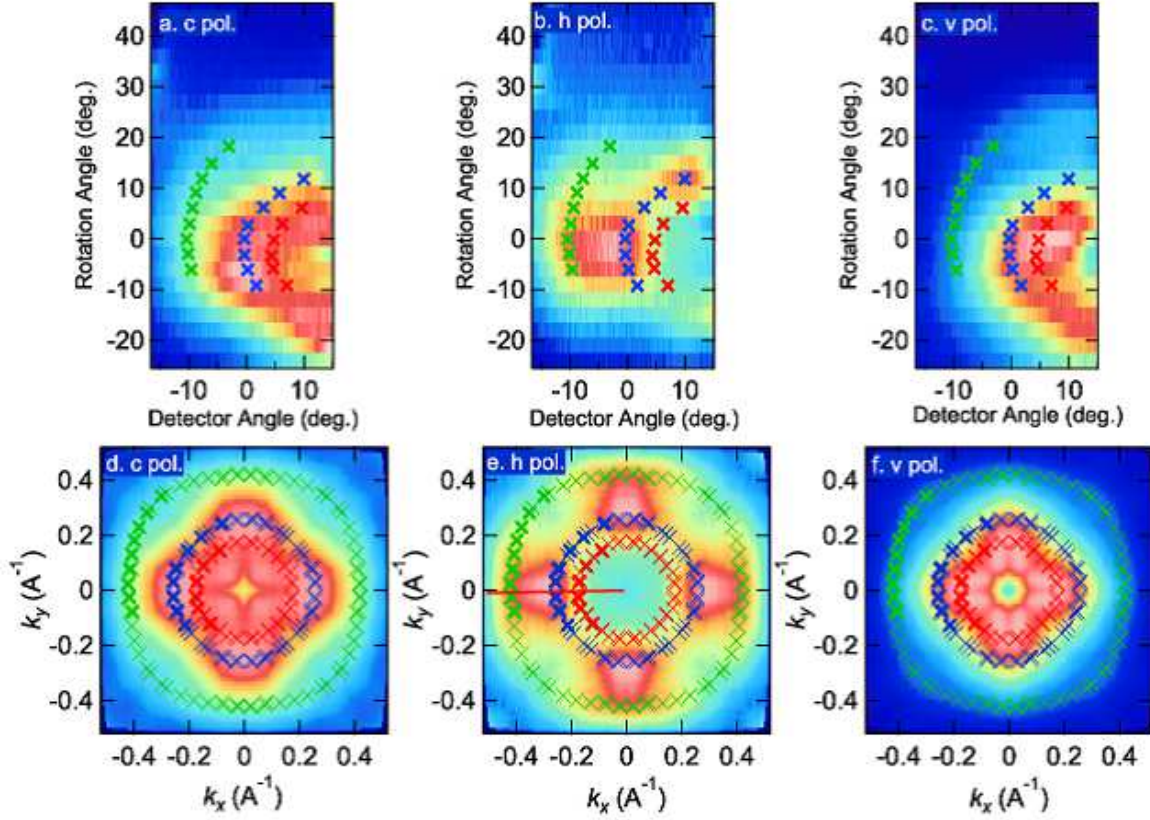


FIG. S 4: Polarization dependence of the FS map for BaK0.76. (a)-(c) Raw FS images plotted with respect to detector and rotation angles measured with c -, h -, and v -polarized light, respectively, and (d)-(f) momentum-mapped FS images.

* Present address: Department of Physics, University of Tokyo, Tokyo 113-0033, Japan

† Present address: Japan Synchrotron Radiation Research Institute (JASRI/SPring-8), Sayo, Hyogo 679-5198, Japan

‡ Present address: Department of Applied Physics, University of Tokyo, Tokyo 113-8656, Japan

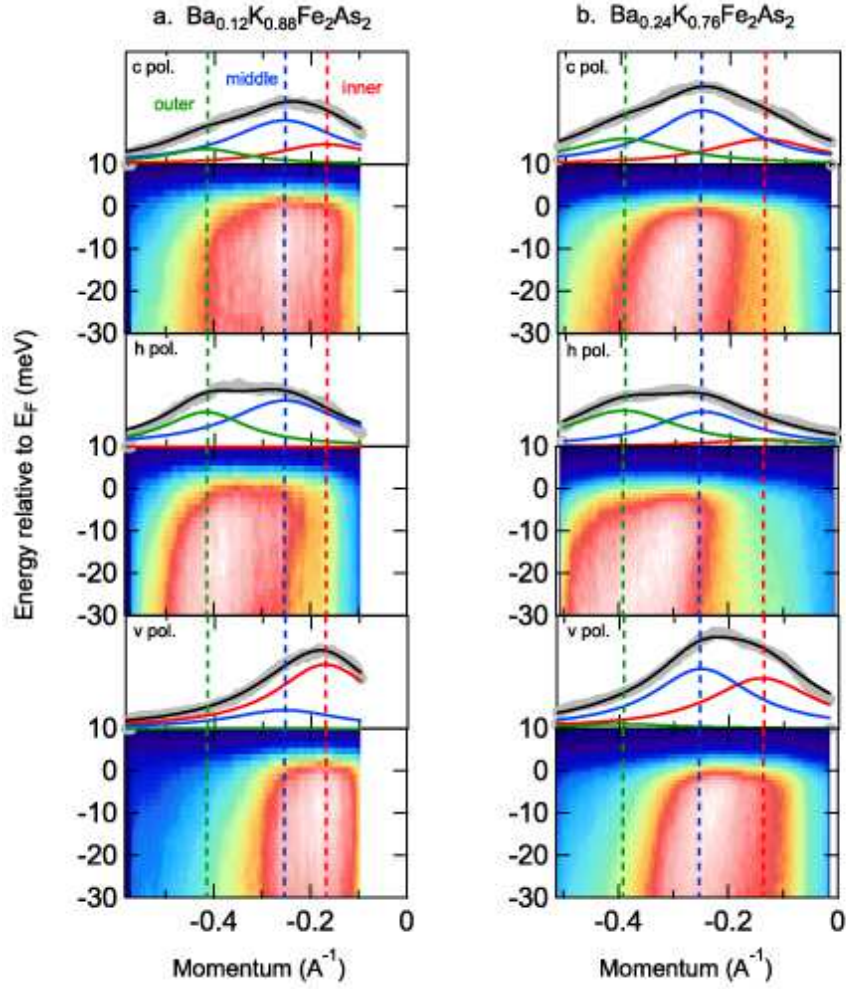


FIG. S 5: MDCs at E_F and E - k maps for BaK0.88 and BaK0.76. (a),(b) MDCs at E_F and E - k maps for BaK0.88 (a) and BaK0.76 (b), respectively, obtained with c -, h -, v -polarized light for FS angle $\varphi \sim 0^\circ$.

$\text{Ba}_{0.24}\text{K}_{0.76}\text{Fe}_2\text{As}_2$ ($T_c \sim 17$ K)

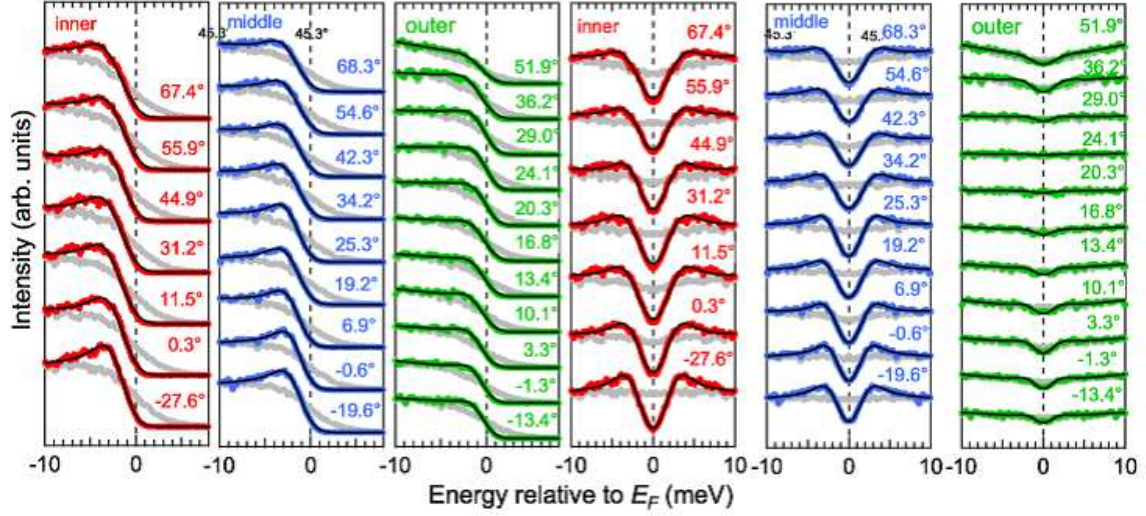


FIG. S 6: EDCs and symmetrized EDCs at k_F below T_c and above T_c for BaK0.76. (a)-(c) EDCs at k_F of inner, middle, and outer FSs, respectively, measured at 1.5 K and 18 K ($T_c \sim 17$ K) for various FS angles as shown in each panel. (d)-(f) Symmetrized EDCs of inner, middle and outer FSs, respectively. Gray markers indicate the EDCs above T_c and the solid lines indicate the fitting functions using a BCS spectral function.

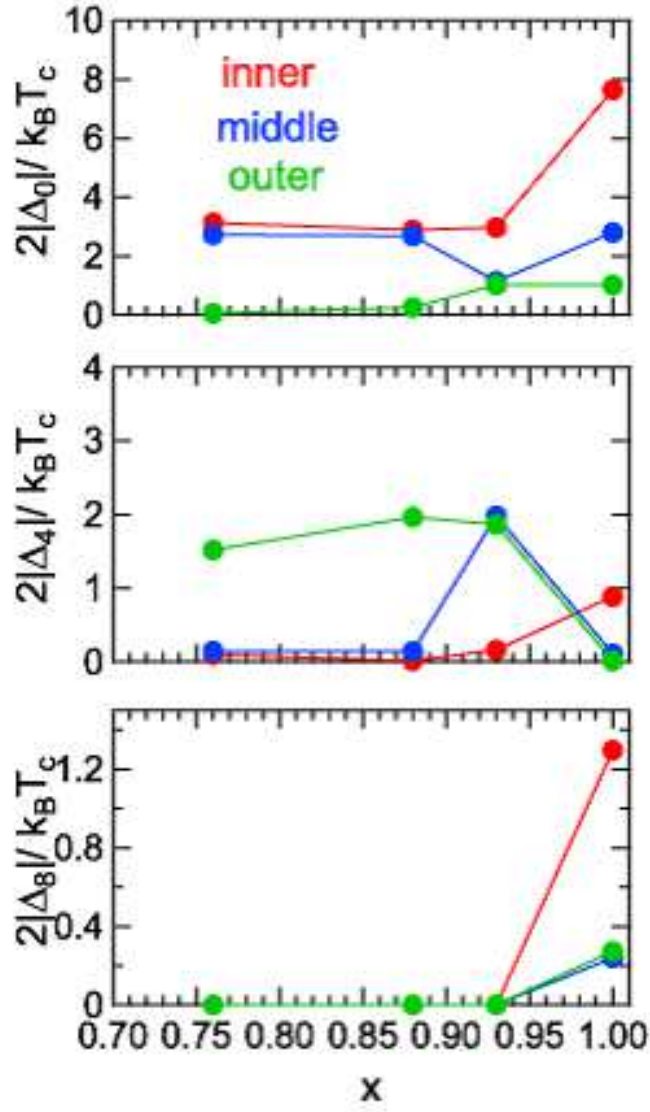


FIG. S 7: Doping dependence of the $2\Delta/k_B T_c$. (a) $2\Delta_0/k_B T_c$ of inner, middle and outer FS, respectively. (b) $2\Delta_4/k_B T_c$ of inner, middle and outer FS, respectively. (c) $2\Delta_8/k_B T_c$ of inner, middle and outer FS, respectively.